THE ASTROPHYSICAL JOURNAL, 460:284–294, 1996 March 20

THE O/H DISTRIBUTION IN THE LOW-MASS GALAXIES NGC 2366 AND NGC 4395

JEAN-RENÉ ROY
Observatoire du mont Mégantic and Université Laval, Département de Physique, Québec, QC G1K 7P4, Canada;
jrroy@phy.ulaval.ca

JULIEN BELLEY
Centre Universitaire St-Louis Maillet, Université de Moncton, Edmunston, NB E3V 2S8, Canada;
jbelley@cslm.ca

YVAN DUTIL
Observatoire du mont Mégantic and Université Laval, Département de Physique, Québec, QC G1K 7PK, Canada;
dutil@phy.ulaval.ca

AND

PIERRE MARTIN
Steward Observatory, University of Arizona, Tucson, AZ 85721; pmartin@as.arizona.ca
Received 1995 June 28; accepted 1995 September 26

ABSTRACT

Results of a spectrophotometric survey in the magellanic barred galaxy NGC 2366 and in the small weakly barred spiral galaxy NGC 4395, employing imaging spectrophotometry with narrow-band interference filters in the lines of Hα, Hβ, [O III] λ5007 and [N II] λ6584, are presented. The use of [O III]/Hβ as an abundance indicator is assessed; it is shown that for the probable range of the physical properties of the H II regions in NGC 2366 and NGC 4395, [O III]/Hβ may not give reliable estimates of O/H abundances in the interstellar gas in these two low-mass galaxies. Instead we use [N II]/[O III], which is more dependable at relatively low abundances. The derived mean levels of O/H (± 1 σ dispersion) in NGC 2366 and NGC 4395 are $12 + \log \mathrm{O/H} = 8.19 \pm 0.14$ and 8.33 ± 0.25, respectively; the global gradients of both galaxies are *flat*. Mechanisms which could explain the absence of abundance gradients in low-mass and irregular galaxies are explored.

Subject headings: galaxies: abundances — galaxies: individual (NGC 2366, NGC 4395) — galaxies: ISM — H II regions

1. INTRODUCTION

Abundance gradients, as mapped from H II region emission-line ratios, are a well established feature of galactic disks (Pagel & Edmunds 1981; Díaz 1989; Dinerstein 1990; Shields 1990; Belley & Roy 1992; Vila-Costas & Edmunds 1992; Zaritsky, Kennicutt, & Huchra 1994; Martin & Roy 1994; Henry & Howard 1995). From the best existing data set of six large disk galaxies (M33, M101, NGC 628, NGC 2997, NGC 6946, and the Milky Way), which have had their O/H gradients derived from samples of ≥ 50 H II regions per galaxy, Belley & Roy (1992) concluded that the gradients in large late-type spirals show identical global slopes of $\sim 0.08 \pm 0.03$ dex kpc^{-1} within the uncertainties. Henry & Howard (1995) also demonstrate that the radial trends of various line ratios in M33, M81, and M101 are matched using exponential abundance gradients with *contant* slopes across their disks.

The abundance of O/H is known to increase with surface brightness in the disks and to diminish as the gas/mass surface density increases (Webster & Smith 1983; Edmunds & Pagel 1984; McCall, Rybsky, & Shields 1985; Ryder 1995). Oey & Kennicutt (1993) have presented evidence that early-type disk galaxies have more metals than late-type galaxies and that their gradients may be flatter. Shallow gradients (e.g., ≤ 0.03 dex kpc^{-1}) are also found in large *barred* galaxies; this was inferred some time ago by Pagel et al. (1979) and Vila-Costas & Edmunds (1992) and recently proved by Martin (1992), Martin & Roy (1994, 1995), and Zaritsky et al. (1994). Martin & Roy have demonstrated further the influence of bars on galactic chemical evolution by showing that *the stronger the "ellipticity" of the bar, the flatter the global O/H gradient*. These findings suggest that bar-shaped magellanic irregulars should have very shallow abundance gradients.

On the other hand, Edmunds & Roy (1993) have suggested that steep abundance gradients in gas-rich galaxies require the presence of unbarred spiral structure; they also remarked that abundance gradients disappear at the same absolute magnitude of which spiral structure ceases. Hence, the occurrence of spiral structure (without a strong bar) and the presence of an abundance gradient would be linked.

Although H II regions have been studied in several dwarf irregular, and blue compact galaxies (see Skillman et al. 1994, and references therein), little is known about chemical variations across these systems (see the works on NGC 5253 by Walsh & Roy 1989b and on II Zw 40 by Walsh & Roy 1993), but these objects are so small that it is difficult to draw conclusions about gradients. Dufour (1986) has already remarked that variations of O/H from one region to another in irregular galaxies are small. The Magellanic Clouds have been studied more successfully, and the data presented by Pagel et al. (1978) are consistent with no gradient. NGC 6822 is another magellanic galaxy in which the few measurements appear consistent with a flat or very shallow gradient (Pagel, Edmunds, & Smith 1980).

In this paper, we present the results of imaging spectrophotometry of two galaxies, NGC 2366 and NGC 4395, which are midway in mass and in luminosity between the large spirals at one end, and the dwarf galaxies at the other end.

2. OBSERVATIONS

NGC 2366 is a SBm IV–V magellanic irregular with an absolute magnitude $M_B = -16.73$ (Wevers, van der Kruit, & Allen 1986). NGC 2366 does not show any spiral pattern; with an inclination angle of 65°, it is similar to the LMC in several of its properties and overall appearance. NGC 2366 possesses a well-studied large H II complex in its southwestern part that is bright enough to have its own NGC number (NGC 2363); Kennicutt, Balick, & Heckman (1980), Peimbert, Pena, & Torres-Peimbert (1986), and González-Delgado et al. (1994) have studied its chemistry and structure, and Roy et al. (1991, 1992) have studied the kinematics and dynamics of the unusual H II region. Wevers et al. (1986) conducted radio observations of the galaxy as part of the Palomar-Westerbork survey of nearby galaxies. We adopt a distance of 3.7 Mpc as proposed by Roy et al. (1992).

NGC 4395 is a small late-type (Sd III–IV) barred galaxy with the stellar bar axis ratio $b/a = 0.35$ (Martin 1995). Very few studies have been published on this galaxy. This emphasizes the unfortunate fact that low surface brightness galaxies have not attracted much attention until recently (see McGaugh 1994). McCall (1992) alluded to the possibility that the abundances in this galaxy may show an unusual behavior. This galaxy is also part of the Palomar-Westerbork survey by Wevers et al. (1986). The spiral pattern is barely traceable. The disk is dominated by a few giant H II complexes which have their own NGC numbers (NGC 4399, NGC 4400, and NGC 4401). NGC 4395 contains a Seyfert 1 nucleus (Filippenko & Sargent 1989). Its distance is uncertain; McCall (1982) quotes a value of 1.85 Mpc, Tully (1988) gives 3.6 Mpc, and Wevers et al. (1986) adopted 4.5 Mpc on the basis of $H_0 = 75$ km s^{-1} Mpc^{-1}; this is the value we have adopted. Its absolute magnitude is $M_B = -18.57$ (Wevers et al. 1986). Its spiral class is 1 on the scale 1–12 defined by Elmegreen & Elmegreen (1987), which corresponds to chaotic and poorly developed arms. The main parameters of the two galaxies are listed in Table 1. $R_{\rm eff}$ is the normalizing radius; it corresponds to half of the effective aperture diameter A_e, which transmits half the total flux from the galaxy as given in de Vaucouleurs et al. (1991).

We obtained monochromatic images of NGC 2366 and NGC 4395 employing a focal reducer on the Mont Mégantic Obervatory 1.6 m telescope. A set of narrow-band ($\Delta\lambda = 10$ or 20 Å) interference filters was used to image the galaxies in the nebular lines of [O III] λ5007, [N II] λ6584, Hα, and Hβ. Two filters with $\Delta\lambda = 200$ Å bandpass, centered at 5370 and 7020 Å, were used to derive the contribution of the red and visual stellar continua. Table 2 lists the exposure times and the interference filters used; these were tilted, dependent on outdoor temperatures, to be tuned to the redshifted nebular line of interest. The detectors used were an RCA 320 × 512 CCD and a Thomson 1024 × 1024 CCD, giving fields of view, respectively, of approximately 6 × 9 arcmin^2 and 10 × 10 arcmin^2 and a pixel size 1.″1 and 0.″7. The sky conditions were generally excellent for the observations of NGC 4395 for NGC 2366, but some of the images of the latter were obtained with the telescope focus slightly off; the seeing was about 2″.

TABLE 1

GLOBAL PROPERTIES OF NGC 2366 AND NGC 4395

Parameter	NGC 2366	NGC 4395
α(2000)[a]	7^{h}28^{m}54^s.4	12^{h}25^{m}49^s.9
δ(2000)[a]	69°12′52″	33°32′46″
Inclination[b]	65°	41°
Position angle[b]	40°	147°
Morphological type[c]	SBm IV–V	Sd III–IV
B_T (mag)[c]	11.46	10.69
A_B (mag)[a]	0.18	0.01
$M^{0,i}_{B_T}$[c]	−16.73	−18.57
Systemic velocity (km s^{-1})[b]	98	330
D(Mpc)	3.7[d]	4.5[b]
$R_{\rm eff}$[a]	128″	172″
Scale (pc arcsec^{-1})	18	22

[a] de Vaucouleurs et al. 1991.
[b] Wevers et al. 1986.
[c] Sandage & Tammann 1981.
[d] Roy et al. 1992.

TABLE 2

JOURNAL OF OBSERVATIONS

Galaxy	Period	Line	Filter (Å)	FWHM (Å)	Integration time (s)
NGC 4395...	1991 Apr 17	Hα	6576	10	3 × 2000
	1991 Apr 17	Hβ	4872	10	4 × 3000
	1991 Apr 18	[O III]	5017	10	3 × 2000
	1991 Apr 18	Visual	5370	200	3 × 500
	1991 Apr 19	Red	7020	200	3 × 500
	1991 Apr 19	[N II]	6002	10	3 × 3000
NGC 2366...	1991 Feb 14	Hα	6577	10	3 × 3000
	1991 Feb 17	Hβ	4872	10	5 × 4000
	1993 Dec 9	[N II]	6602	9	3 × 2000
	1991 Feb 14	[O III]	5019	20	3 × 2000
	1991 Feb 18	Visual	5370	200	3 × 500
	1991 Feb 18	Red	7020	200	3 × 500

3. RESULTS

Figure 1 (Plates 5–6) shows images of NGC 2366 in the light of Hα and of the red continuum. Figure 2 (Plates 7–8) shows images of NGC 4395 for the same bandpasses. All image reduction procedures were done with the NOAO IRAF image analysis software; these procedures have been described in detail in Belley & Roy (1992) and Martin & Roy (1992, 1994). Flux calibrations were done the following way: For NGC 2366, we used an average of line ratios from two long-slit spectra obtained with the MOS spectrograph at CFHT of regions 22 and 30 (Fig. 3*a* [Pl. 9] and Table 3) and the spectroscopic data from Peimbert et al. (1986) on the giant H II region NGC 2363 (region 24 in Fig. 3*a*); an aperture of the same size (3.6 × 11 arcsec^2) as the slit used by Peimbert et al. was defined on our images and counts were measured in that aperture. For NGC 4395, we used the spectrophotometric data of three bright H II regions of NGC 4395 in common with McCall et al. (1985); those regions are identified as numbers 2, 15, and 42 in Figure 3*b* (Plate 10) and Table 4. However, it should be noted that we had difficulty matching with certainty the regions studied by McCall et al. because the regions appear, seen in the continuum, as a cluster of several knots. Region 2, close to the center of the galaxy, could be contaminated by the nuclear activity (Filippenko & Sargent 1989).

Imaging spectrophotometry with narrow-band filters allows us to obtain flux measurements in a few spectral elements, but for a large number of objects in the field. A clear advantage is that one measures fluxes integrated over

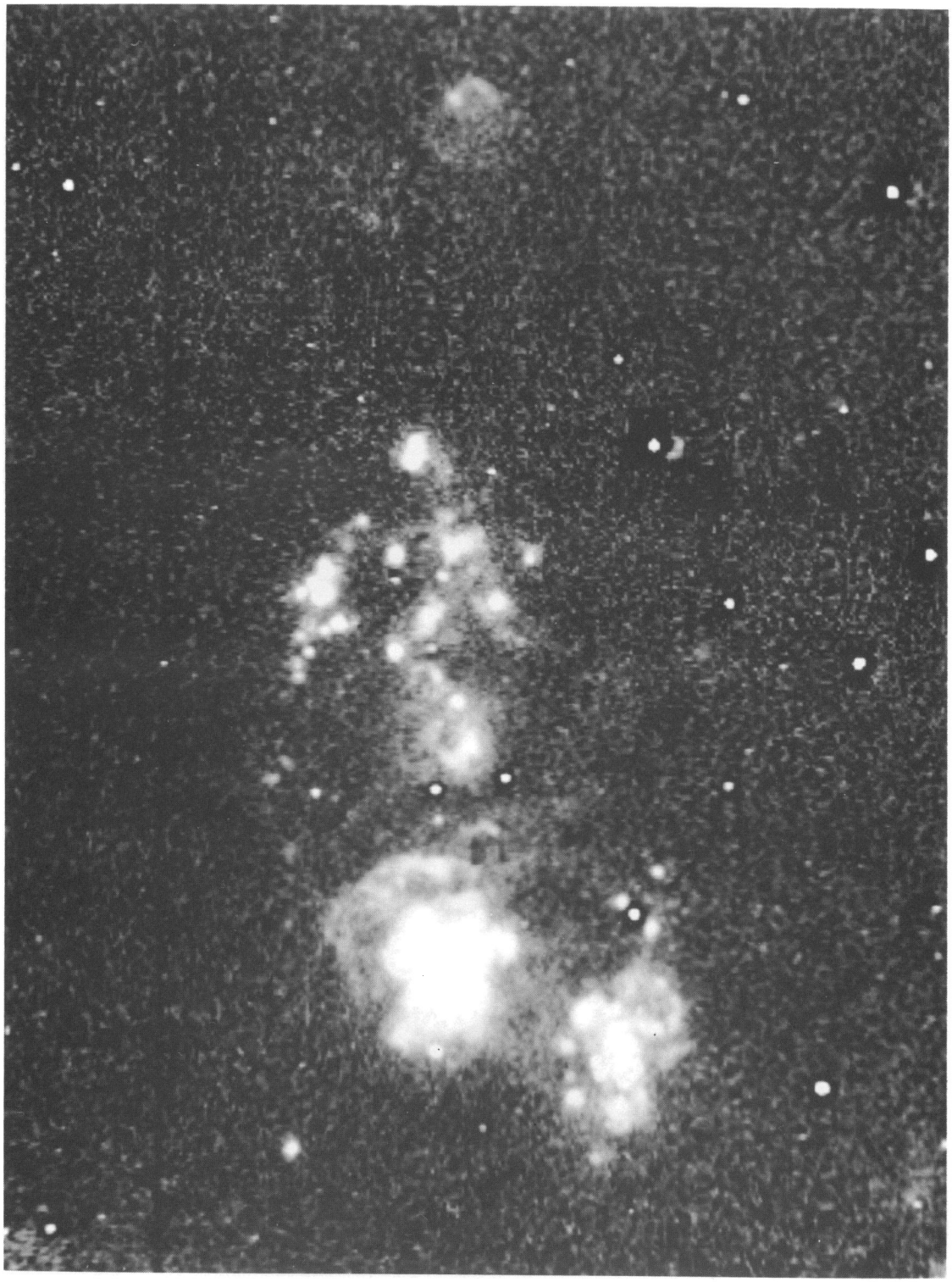

FIG. 1*a*

FIG. 1.—Images of the galaxy NGC 2366 obtained with a focal reducer at Mont Mégantic Observatory. (*a*) Hα and (*b*) red continuum images. North is at 35° counterclockwise from the top, and east is roughly at left. The field of view of ≈5.8 × 7.7 arcmin^2. The circle is the photometric center given by Dressel & Condon (1976). The images were obtained under poor seeing conditions.

PLATE 6

FIG. 1*b*

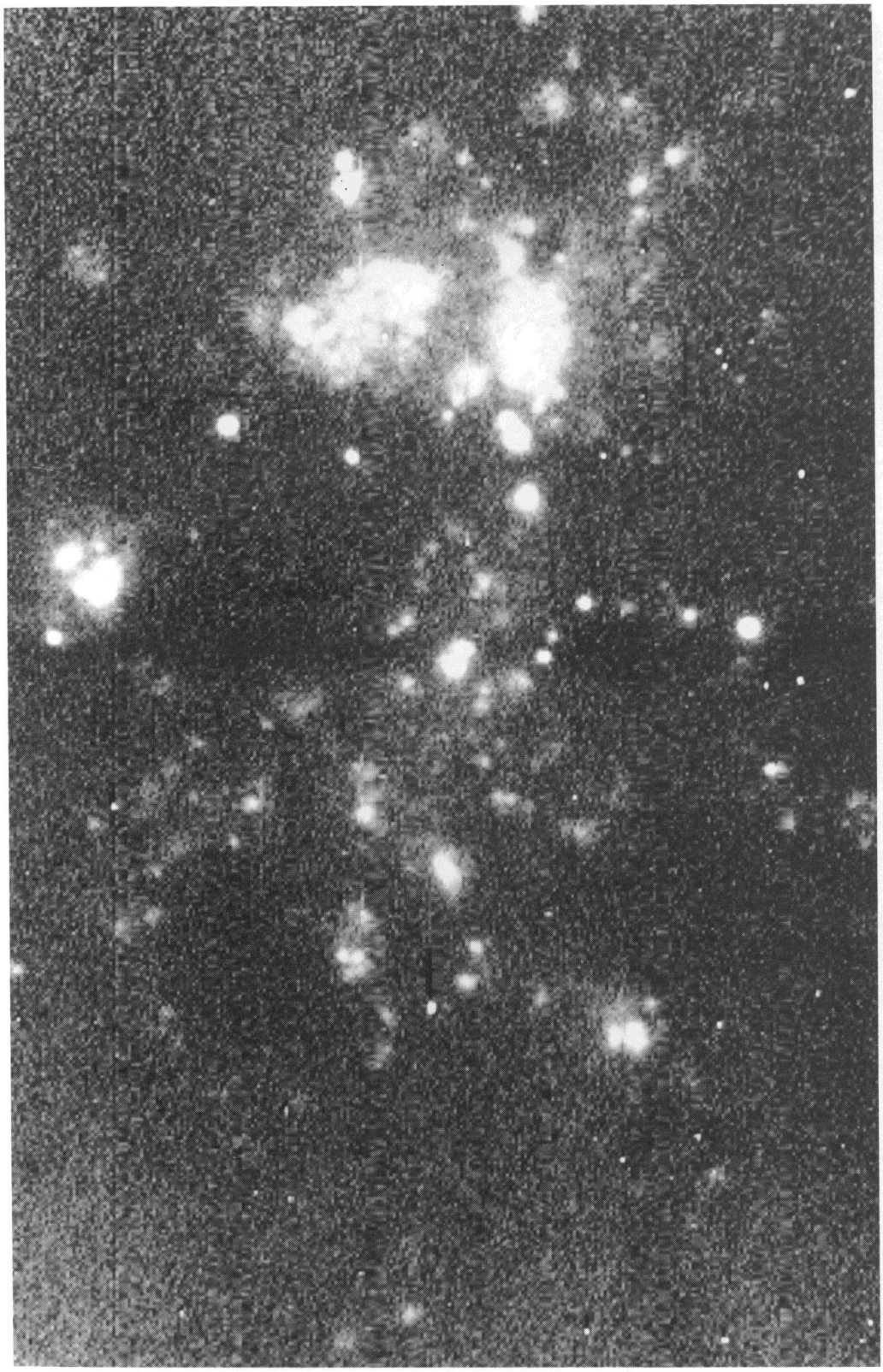

FIG. 2a

FIG. 2.—Images of the galaxy NGC 4395 with the same set-up as in Figure 1. (*a*) Hα and (*b*) red continuum. North is at the top, and east is at the left. The field of view is 5.3 × 8.5 arcmin^2.

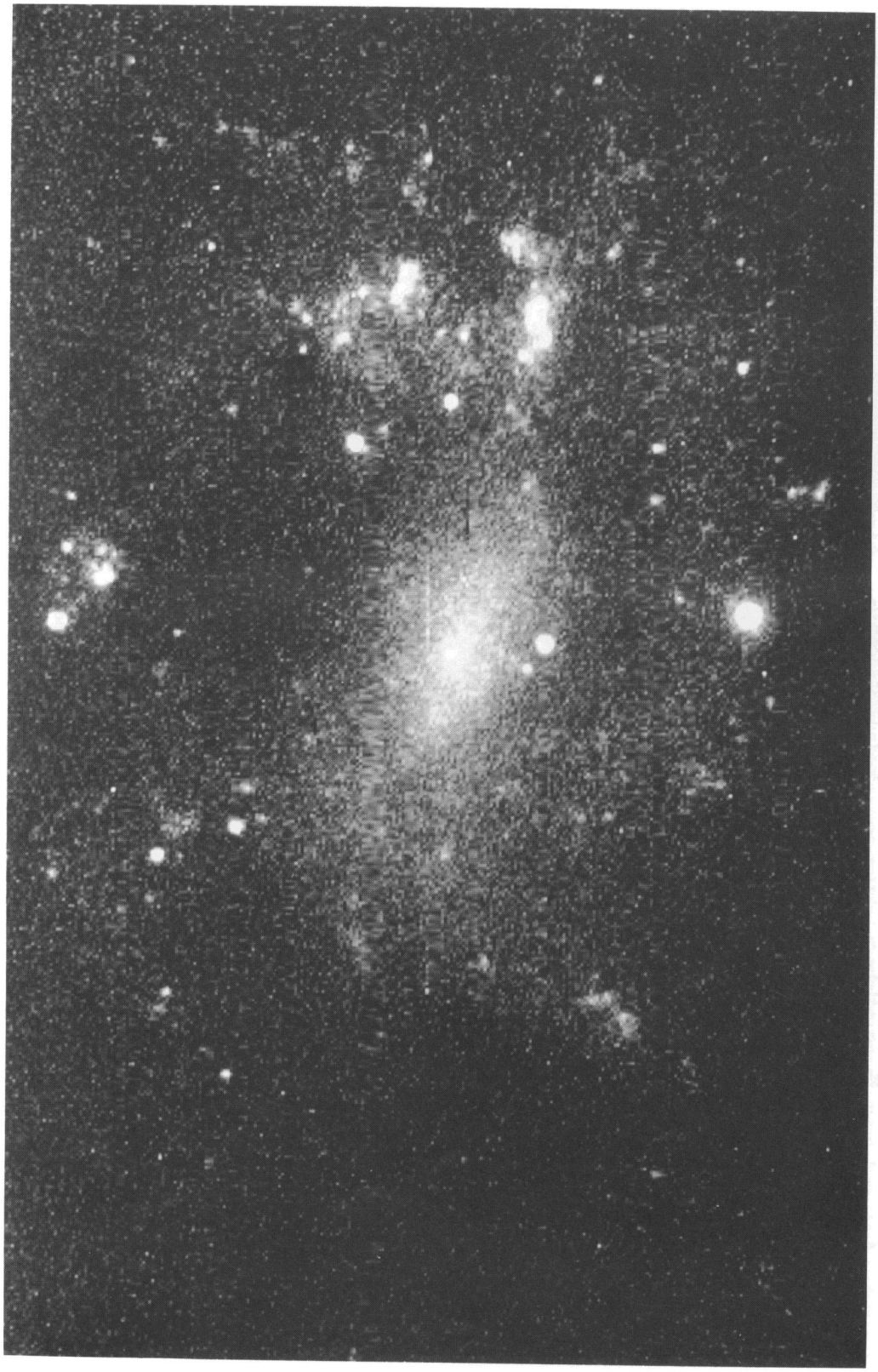

FIG. 2*b*

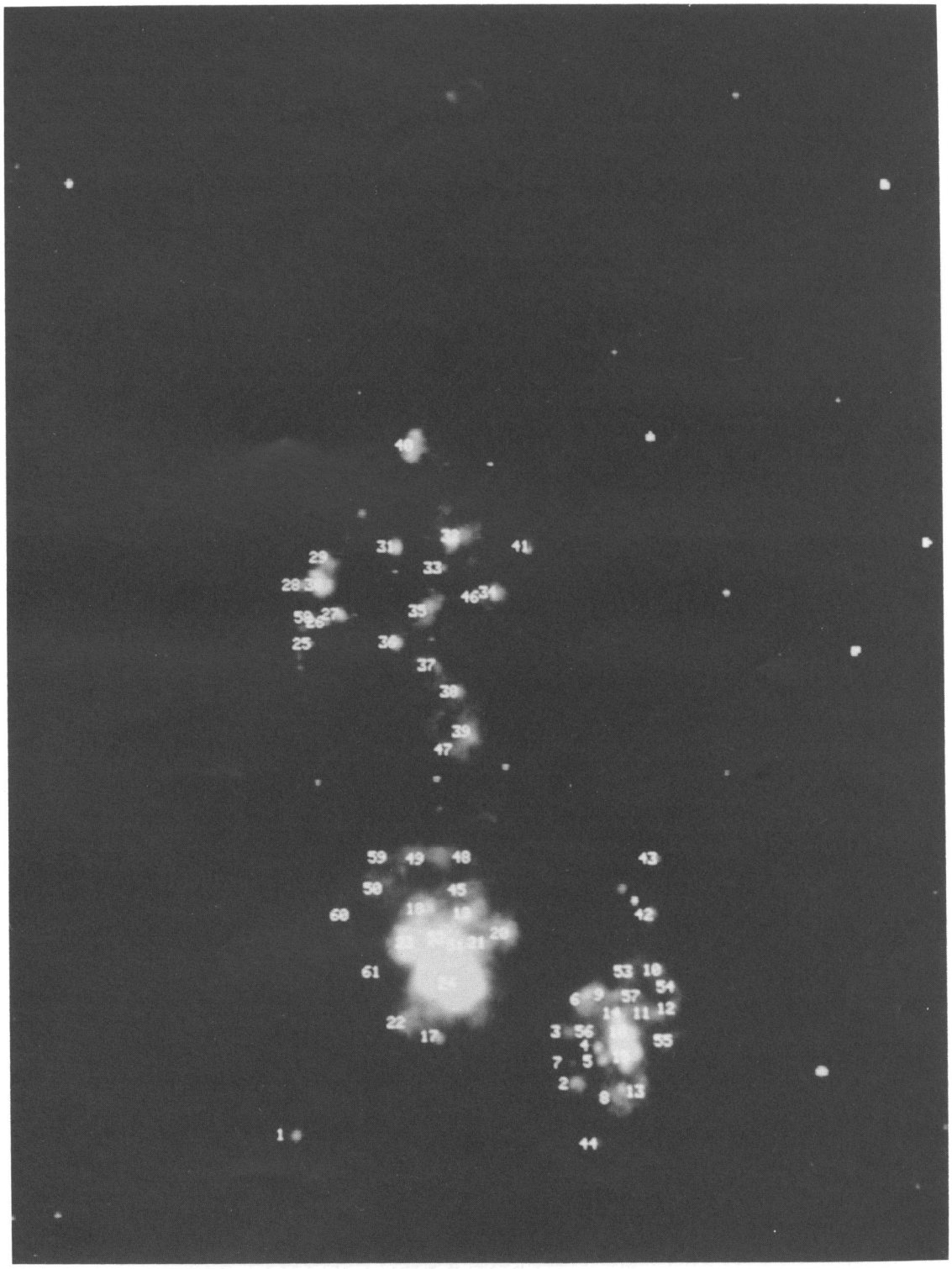

FIG. 3*a*

FIG. 3.—Hα images of (*a*) NGC 2366 and (*b*) NGC 4395 with the identification of the H II regions whose nebular fluxes were measured with the required level of S/N.

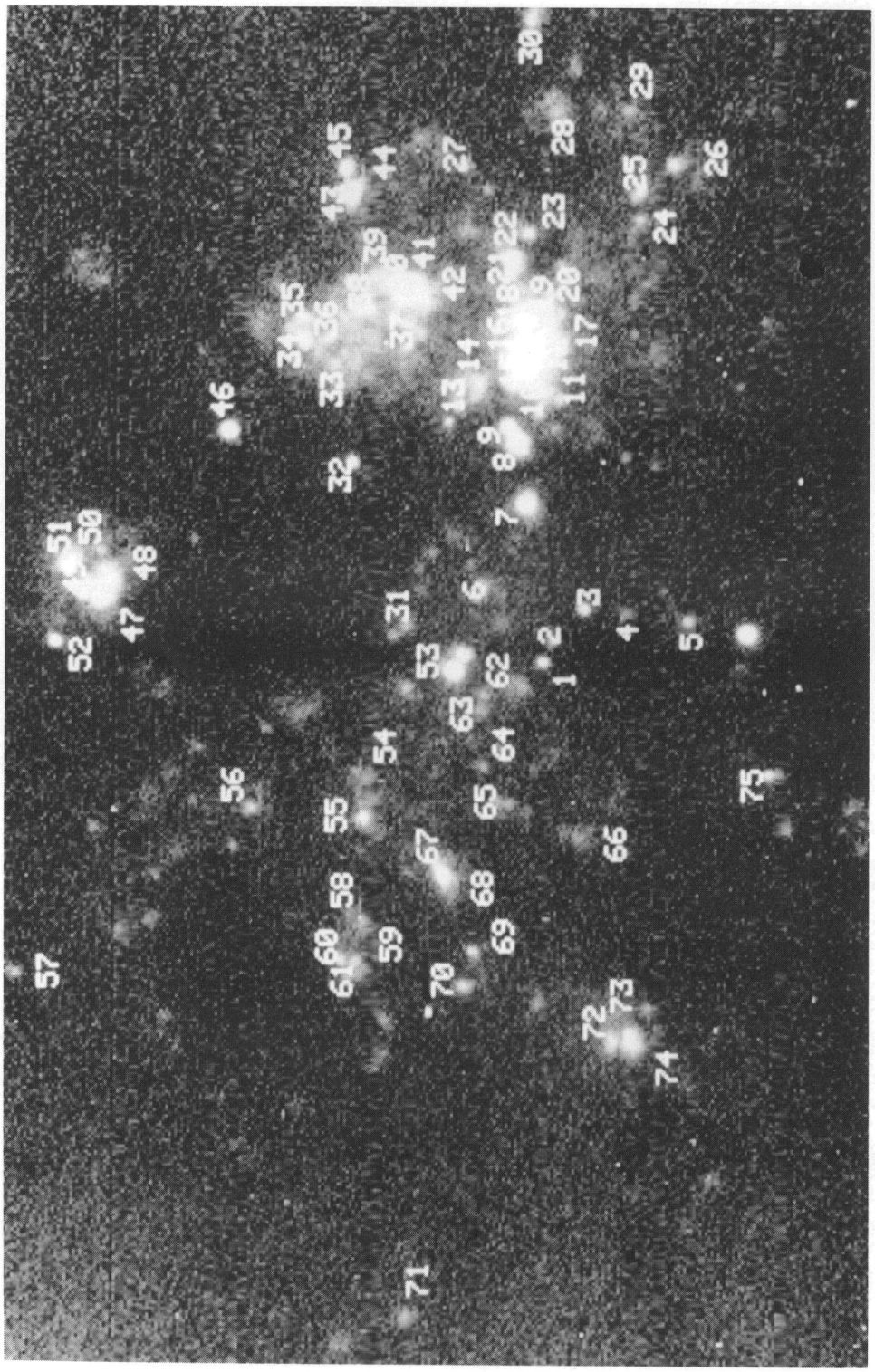

FIG. 3*b*

the whole area of individual H II regions. Comparison can be made more directly with nebular line ratios predicted from photoionization models because models assume that one measures fluxes integrated over the whole nebular volume. An inconvenience is the difficulty of subtracting accurately the underlying continuum; because a broadband filter positioned at several hundred Å from the nebular lines of interest is usually used for the subtraction, uncertainties can be large, especially for lines which are a few Å in equivalent width. In addition, the difficulty is increased for a line like [N II] in the low-mass galaxies which is weak and close to the bright Hα emission line; this necessitates careful tuning of the filters and stiff rejection criteria; in our case, we apply a cutoff on equivalent width and reject regions close to foreground stars. Nevertheless, the method is most useful when used jointly with conventional spectroscopy, it provides a powerful tool for investigating the chemical composition of galaxies.

Integrated nebular fluxes were derived for 61 H II regions in NGC 2366 and 75 H II regions in NGC 4395; the regions are identified in Figures 3*a* and 3*b*, and their positions are given in Tables 3 and 4; positive numbers represent east and north direction from the nucleus in NGC 4395 and from the photometric center in NGC 2366. The main criteria for retention of an H II region were that its emission-line equivalent width at Hβ be about 10 or greater, and any considered line ratio have a signal-to-noise ratio larger than 5. The various errors and uncertainties inherent to the several steps of image reduction and calibration have been discussed extensively in Belley & Roy (1992), and Scowen, Dufour, & Hester (1992).

The flux values were corrected for interstellar reddening by comparing the Hα/Hβ ratios to the theoretical Balmer decrement (case B) as given by Brocklehurst (1971) for a density of 100 cm^{-3} and a temperature of 10,000 K. The redening correction was applied using the reddening law of Savage & Mathis (1979). Because of the small redshift of the galaxies, reddening was calculated directly from the observed Hα/Hβ ratio; the reader is again referred to Belley & Roy (1992) for more details. The corrected line ratios listed in Tables 5 and 6 were calculated by finding the ratio of the integrated flux over each region after correction for interstellar reddening. For consistency with other published spectrophotometric works, the ratio [O III]/Hβ is defined as 1.35 I([O III] λ5007)/Hβ as in McCall et al. (1985), and [N II]/[O III] as I([N II] λ6584)/I([O III] λ5007).

Because of the difficulty in defining a normalizing radius in low-mass galaxies, we used the deprojected linear distance in kiloparsecs to the galaxy center. The strong inclination and the lack of a nucleus in NGC 2366 are sources of uncertainty in the deprojection; deprojection was done assuming a flat system, $i = 65°$ and P.A. = 40° (Wevers et al. 1986). The radial distances in NGC 2366 are from the photometric center as defined by Dressel & Condon (1976); this center is marked by a circle on the red continuum image of NGC 2366 (Fig. 1*b*).

We inferred A_v from the logarithmic extinction at Hβ assuming $R = 3.2$. One notes the relatively high value of

TABLE 3

H II Region Identification in NGC 2366

Region	X	Y	Region	X	Y
1	−38	−148	32	33	66
2	−114	−74	33	33	52
3	−102	−60	34	10	58
4	−113	−58	35	28	36
5	−117	−62	36	31	21
6	−101	−46	37	14	22
7	−108	−60	38	2	19
8	−130	−69	39	−10	9
9	−107	−40	40	67	83
10	−117	−22	41	10	78
11	−123	−38	42	−103	−7
12	−129	−31	43	−93	10
13	−136	−62	44	−132	−87
14	−114	−44	45	−41	−39
15	−125	−55	46	15	52
16	−119	−48	47	−8	0
17	−62	−89	48	−36	−28
18	−32	−54	49	−22	−39
19	−47	−45	50	−15	−56
20	−63	−43	51	−52	−56
21	−58	−51	52	−44	−58
22	−49	−92	53	−109	−29
23	−36	−66	54	−125	−25
24	−57	−70	55	−13	−41
25	57	2	56	−109	−55
26	58	12	57	−116	−35
27	54	17	58	62	10
28	72	18	59	−10	−46
29	70	32	60	−10	−71
30	66	22	61	−32	−82
31	51	49			

TABLE 4

H II Region Identification in NGC 4395

Region	X	Y	Region	X	Y
1	0	0	39	−32	134
2	3	4	40	−39	144
3	31	23	41	−29	146
4	48	18	42	−17	143
5	85	30	43	−37	176
6	10	61	44	−36	179
7	26	86	45	−40	187
8	23	90	46	−81	89
9	20	96	47	−127	28
10	30	101	48	−125	35
11	37	102	49	−134	26
12	32	100	50	−132	32
13	1	108	51	−128	43
14	9	111	52	−140	39
15	24	122	53	−18	−8
16	28	118	54	−35	−39
17	35	128	55	−33	−55
18	29	133	56	−74	−53
19	37	140	57	−157	−113
20	34	149	58	−33	−94
21	21	154	59	−35	−109
22	21	152	60	−41	−108
23	39	162	61	−37	−116
24	26	168	62	24	−7
25	67	179	63	11	−10
26	67	190	64	10	−15
27	79	208	65	15	−50
28	36	209	66	45	−63
29	63	242	67	−7	−75
30	26	15	68	−3	−77
31	−18	113	69	7	−106
32	−43	123	70	3	−118
33	−55	127	71	−18	−239
34	−59	131	72	57	−138
35	−55	123	73	64	136
36	−46	130	74	65	−140
37	−23	134	75	114	−41
38	−35	134			

TABLE 5

PROPERTIES OF H II REGIONS IN NGC 2366

	LOG OF CORRECTED LINE RATIOS				PROPERTIES	
REGION	[O III]/Hβ	[N II]/[O III]	[N II]/Hα	R_{kpc}	c(Hβ)	O/H
1	0.69 ± 0.03	−1.81 ± 0.03	−1.83 ± 0.01	6.46	0.19 ± 0.05	8.19
2	0.78 ± 0.02	−1.86 ± 0.01	−1.79 ± 0.01	4.72	0.08 ± 0.03	8.17
3	0.45 ± 0.04	−1.63 ± 0.04	−1.88 ± 0.01	4.00	0.05 ± 0.04	8.27
4	0.78 ± 0.02	−1.92 ± 0.01	−1.85 ± 0.01	4.15	0.09 ± 0.03	8.13
5	0.65 ± 0.02	−1.83 ± 0.02	−1.89 ± 0.01	4.36	0.01 ± 0.03	8.18
6	0.67 ± 0.01	−1.74 ± 0.01	−1.78 ± 0.00	3.50	0.09 ± 0.02	8.22
7	0.61 ± 0.05	−1.73 ± 0.04	−1.73 ± 0.02	4.44	−0.25 ± 0.08	8.23
8	0.33 ± 0.02	−1.49 ± 0.02	−1.86 ± 0.01	4.84	0.00 ± 0.02	8.31
9	0.51 ± 0.02	−1.56 ± 0.02	−1.76 ± 0.01	3.41	0.13 ± 0.03	8.29
10	0.62 ± 0.04	−1.71 ± 0.03	−1.80 ± 0.01	3.06	0.26 ± 0.06	8.24
11	0.65 ± 0.01	−1.74 ± 0.01	−1.80 ± 0.01	3.63	0.04 ± 0.02	8.22
12	0.63 ± 0.02	−1.70 ± 0.02	−1.74 ± 0.01	3.56	−0.10 ± 0.04	8.24
13	0.26 ± 0.03	−1.42 ± 0.03	−1.83 ± 0.01	4.71	−0.10 ± 0.03	8.33
14	0.53 ± 0.01	−1.61 ± 0.01	−1.79 ± 0.00	3.66	0.12 ± 0.02	8.27
15	0.68 ± 0.00	−1.81 ± 0.00	−1.84 ± 0.00	4.25	0.20 ± 0.01	8.19
16	0.79 ± 0.00	−1.90 ± 0.00	−1.81 ± 0.00	3.91	0.22 ± 0.01	8.14
17	0.77 ± 0.02	−1.85 ± 0.02	−1.79 ± 0.01	4.44	0.26 ± 0.04	8.17
18	0.80 ± 0.01	−1.90 ± 0.00	−1.81 ± 0.00	2.59	0.15 ± 0.01	8.14
19	1.05 ± 0.00	−2.11 ± 0.00	−1.77 ± 0.00	2.50	0.13 ± 0.01	7.98
20	1.14 ± 0.01	−2.20 ± 0.00	−1.77 ± 0.00	2.69	0.10 ± 0.02	7.88
21	1.15 ± 0.01	−2.22 ± 0.00	−1.77 ± 0.00	2.89	−0.01 ± 0.02	7.86
22	0.60 ± 0.01	−1.68 ± 0.01	−1.79 ± 0.00	4.36	0.22 ± 0.02	8.25
23	0.91 ± 0.00	−2.03 ± 0.00	−1.83 ± 0.00	3.13	0.26 ± 0.00	8.05
24	1.15 ± 0.00	−2.24 ± 0.00	−1.80 ± 0.00	3.60	0.27 ± 0.00	7.85
25	0.74 ± 0.05	−1.74 ± 0.04	−1.71 ± 0.02	1.27	0.10 ± 0.09	8.22
26	0.45 ± 0.06	−1.59 ± 0.06	−1.85 ± 0.02	1.52	0.26 ± 0.07	8.28
27	0.65 ± 0.02	−1.74 ± 0.02	−1.80 ± 0.01	1.62	0.23 ± 0.03	8.22
28	0.49 ± 0.04	−1.71 ± 0.04	−1.93 ± 0.01	2.00	0.21 ± 0.05	8.24
29	0.43 ± 0.03	−1.49 ± 0.02	−1.77 ± 0.01	2.41	0.18 ± 0.03	8.31
30	0.73 ± 0.01	−1.94 ± 0.01	−1.92 ± 0.00	2.01	0.20 ± 0.01	8.11
31	0.57 ± 0.02	−1.73 ± 0.02	−1.87 ± 0.01	2.72	0.52 ± 0.03	8.23
32	0.77 ± 0.01	−1.98 ± 0.01	−1.91 ± 0.00	3.11	0.23 ± 0.01	8.09
33	0.52 ± 0.06	−1.82 ± 0.06	−2.01 ± 0.02	2.55	0.32 ± 0.08	8.18
34	0.63 ± 0.02	−1.74 ± 0.01	−1.81 ± 0.01	2.43	0.10 ± 0.03	8.22
35	0.28 ± 0.03	−1.52 ± 0.03	−1.94 ± 0.01	1.85	0.07 ± 0.02	8.30
36	0.64 ± 0.01	−1.92 ± 0.01	−1.95 ± 0.01	1.31	−0.11 ± 0.02	8.13
37	0.21 ± 0.07	−1.43 ± 0.07	−1.93 ± 0.01	1.08	0.13 ± 0.05	8.33
38	0.28 ± 0.04	−1.39 ± 0.04	−1.83 ± 0.01	0.79	0.17 ± 0.04	8.33
39	0.76 ± 0.01	−1.88 ± 0.01	−1.83 ± 0.01	0.34	0.22 ± 0.02	8.15
40	0.85 ± 0.01	−2.01 ± 0.01	−1.88 ± 0.00	4.29	0.35 ± 0.02	8.06
41	0.75 ± 0.03	−1.87 ± 0.03	−1.83 ± 0.01	3.27	0.35 ± 0.06	8.16
42	0.49 ± 0.03	−1.62 ± 0.03	−1.80 ± 0.01	2.38	−0.11 ± 0.04	8.27
43	0.48 ± 0.08	−1.47 ± 0.07	−1.70 ± 0.02	1.83	0.12 ± 0.09	8.31
44	0.59 ± 0.06	−1.69 ± 0.06	−1.81 ± 0.02	5.53	0.07 ± 0.09	8.24
45	0.97 ± 0.01	−2.03 ± 0.01	−1.77 ± 0.01	2.17	0.14 ± 0.02	8.05
46	0.38 ± 0.06	−1.62 ± 0.06	−1.93 ± 0.02	2.28	−0.05 ± 0.06	8.27
47	0.57 ± 0.03	−1.80 ± 0.03	−1.93 ± 0.01	0.17	0.07 ± 0.04	8.20
48	0.77 ± 0.03	−1.85 ± 0.02	−1.76 ± 0.01	1.68	−0.07 ± 0.06	8.17
49	0.60 ± 0.01	−1.69 ± 0.01	−1.80 ± 0.00	1.85	0.24 ± 0.02	8.24
50	0.62 ± 0.02	−1.73 ± 0.02	−1.82 ± 0.01	2.47	0.16 ± 0.03	8.23
51	1.17 ± 0.00	−2.26 ± 0.00	−1.80 ± 0.00	2.99	−0.01 ± 0.01	7.81
52	1.06 ± 0.00	−2.11 ± 0.00	−1.76 ± 0.00	2.95	0.12 ± 0.01	7.98
53	0.63 ± 0.02	−1.76 ± 0.02	−1.84 ± 0.01	3.08	0.10 ± 0.03	8.21
54	0.55 ± 0.05	−1.54 ± 0.04	−1.69 ± 0.01	3.28	0.12 ± 0.06	8.30
55	0.56 ± 0.03	−1.72 ± 0.03	−1.79 ± 0.01	4.00	−0.21 ± 0.04	8.23
56	0.48 ± 0.06	−1.54 ± 0.05	−1.76 ± 0.02	3.95	0.06 ± 0.07	8.29
57	0.74 ± 0.04	−1.91 ± 0.04	−1.85 ± 0.02	3.41	−0.05 ± 0.08	8.14
58	0.46 ± 0.08	−1.66 ± 0.07	−1.91 ± 0.02	1.58	0.23 ± 0.09	8.25
59	0.52 ± 0.06	−1.63 ± 0.05	−1.82 ± 0.02	2.00	0.21 ± 0.08	8.26
60	0.67 ± 0.03	−1.70 ± 0.03	−1.74 ± 0.01	3.01	0.23 ± 0.06	8.24
61	0.47 ± 0.07	−1.60 ± 0.06	−1.84 ± 0.02	3.71	0.11 ± 0.08	8.27

$A_v = 1.12$ with a dispersion of ±0.50 in NGC 4395, most of which is intrinsic since the Galactic component of absorption is small in that direction (Table 1); in NGC 2366, the mean $A_v = 0.30$ with a dispersion of ±0.24 is smaller, most of the extinction being probably Galactic. As for previous works (van der Hulst et al. 1988 on M51, Walsh & Roy 1989a on NGC 2997, Belley & Roy 1992 on NGC 628 and NGC 6946, Martin & Roy 1992 on NGC 4303, and Martin & Roy 1994 on NGC 925 and NGC 1073), *no* significant trend of extinction as a function of galactocentric distance appears to be present when measured from the spectra of H II regions.

TABLE 6

PROPERTIES OF H II REGIONS IN NGC 4395

REGION	LOG OF CORRECTED LINE RATIOS			R_{kpc}	PROPERTIES	
	[O III]/Hβ	[N II]/[O III]	[N II]/Hα		c(Hβ)	O/H
1	0.97 ± 0.00	−1.68 ± 0.00	−0.99 ± 0.00	0.00	0.95 ± 0.01	8.34
2	0.54 ± 0.02	−1.72 ± 0.04	−1.46 ± 0.03	0.13	0.56 ± 0.03	8.30
3	0.52 ± 0.03	...	...	0.89	0.00 ± 0.06	...
4	0.63 ± 0.03	...	...	1.49	0.98 ± 0.07	...
5	0.45 ± 0.07	−1.01 ± 0.05	−0.84 ± 0.02	2.48	1.10 ± 0.13	8.55
6	0.68 ± 0.07	...	...	0.74	0.69 ± 0.14	...
7	0.30 ± 0.02	−1.21 ± 0.02	−1.19 ± 0.02	1.60	0.58 ± 0.03	8.43
8	0.51 ± 0.01	...	...	2.07	0.48 ± 0.03	...
9	0.25 ± 0.02	...	...	2.10	0.54 ± 0.03	...
10	0.26 ± 0.08	...	...	2.37	0.74 ± 0.12	...
11	0.88 ± 0.04	...	...	2.61	0.82 ± 0.09	...
12	0.44 ± 0.02	...	...	2.56	0.32 ± 0.04	...
13	0.20 ± 0.07	...	...	2.22	0.73 ± 0.10	...
14	0.30 ± 0.03	...	...	2.43	0.57 ± 0.05	...
15	0.87 ± 0.00	−2.35 ± 0.02	−1.77 ± 0.02	2.62	0.67 ± 0.01	7.96
16	0.81 ± 0.00	−2.36 ± 0.02	−1.83 ± 0.02	2.88	0.42 ± 0.01	7.87
17	−0.44 ± 0.01	...	...	2.89	0.00 ± 0.01	...
18	0.73 ± 0.00	−2.47 ± 0.01	−2.02 ± 0.01	2.99	0.59 ± 0.00	7.80
19	0.32 ± 0.04	...	...	3.21	0.73 ± 0.07	...
20	0.43 ± 0.04	...	...	3.32	0.65 ± 0.07	...
21	0.40 ± 0.02	...	...	3.38	0.37 ± 0.04	...
22	0.63 ± 0.01	...	...	3.50	0.59 ± 0.02	...
23	0.50 ± 0.05	...	...	3.61	0.33 ± 0.10	...
24	0.53 ± 0.03	−0.79 ± 0.05	−0.54 ± 0.04	3.69	0.55 ± 0.05	8.57
25	0.38 ± 0.07	...	...	4.34	0.70 ± 0.12	...
26	0.35 ± 0.04	...	...	4.59	0.59 ± 0.07	...
27	−0.13 ± 0.09	...	...	4.96	0.81 ± 0.07	...
28	0.48 ± 0.04	...	...	4.81	0.59 ± 0.09	...
29	0.68 ± 0.06	...	...	5.13	0.55 ± 0.12	...
30	0.48 ± 0.05	...	...	5.46	0.73 ± 0.09	...
31	0.52 ± 0.07	...	...	0.55	0.61 ± 0.14	...
32	0.43 ± 0.03	−1.20 ± 0.04	−1.05 ± 0.30	2.65	0.31 ± 0.06	8.41
33	0.45 ± 0.02	...	...	2.96	0.70 ± 0.03	...
34	1.32 ± 0.03	...	...	3.07	0.47 ± 0.08	...
35	0.52 ± 0.03	...	...	3.11	0.63 ± 0.05	...
36	0.34 ± 0.05	...	...	2.87	0.74 ± 0.08	...
37	0.54 ± 0.03	...	...	2.86	0.27 ± 0.06	...
38	0.40 ± 0.03	...	...	3.01	0.48 ± 0.04	...
39	0.43 ± 0.03	−1.03 ± 0.02	−0.88 ± 0.01	2.99	0.84 ± 0.05	8.51
40	0.52 ± 0.04	...	...	3.23	0.56 ± 0.07	...
41	0.65 ± 0.02	...	...	3.23	0.38 ± 0.05	...
42	0.65 ± 0.00	−1.77 ± 0.01	−1.40 ± 0.01	3.13	0.49 ± 0.01	8.27
43	0.75 ± 0.01	...	...	3.90	0.45 ± 0.03	...
44	0.45 ± 0.01	...	...	3.96	0.52 ± 0.03	...
45	0.70 ± 0.01	...	...	4.14	0.73 ± 0.03	...
46	0.65 ± 0.01	...	...	2.82	0.76 ± 0.02	...
47	0.29 ± 0.01	...	...	3.57	0.57 ± 0.02	...
48	0.15 ± 0.03	...	...	3.57	0.63 ± 0.04	...
49	0.73 ± 0.02	...	...	3.81	0.55 ± 0.05	...
50	0.19 ± 0.05	...	...	3.71	0.56 ± 0.07	...
51	0.27 ± 0.07	...	...	3.68	0.69 ± 0.11	...
52	0.37 ± 0.02	...	...	3.98	0.68 ± 0.04	...
53	0.67 ± 0.06	...	...	0.54	0.51 ± 0.13	...
54	0.90 ± 0.07	...	...	1.38	0.61 ± 0.17	...
55	0.61 ± 0.02	...	...	1.74	0.44 ± 0.04	...
56	0.38 ± 0.07	...	...	2.52	0.67 ± 0.12	...
57	0.29 ± 0.08	...	...	5.36	0.39 ± 0.13	...
58	0.33 ± 0.04	...	...	2.40	0.00 ± 0.06	...
59	0.56 ± 0.03	...	...	2.77	0.35 ± 0.06	...
60	0.46 ± 0.04	...	...	2.82	0.38 ± 0.06	...
61	0.81 ± 0.04	...	...	2.91	0.20 ± 0.08	...
62	0.16 ± 0.09	...	...	0.70	0.27 ± 0.11	...
63	0.15 ± 0.08	...	...	0.41	0.23 ± 0.10	...
64	0.86 ± 0.07	...	...	0.47	0.57 ± 0.15	...
65	0.01 ± 0.10	...	...	1.14	0.17 ± 0.10	...
66	0.10 ± 0.10	...	...	1.85	0.07 ± 0.11	...
67	0.64 ± 0.03	...	...	1.68	0.30 ± 0.07	...
68	0.59 ± 0.01	−1.59 ± 0.02	−1.28 ± 0.02	1.68	0.38 ± 0.02	8.32
69	0.66 ± 0.03	...	...	2.30	0.14 ± 0.07	...
70	0.39 ± 0.04	...	...	2.57	0.26 ± 0.07	...
71	0.50 ± 0.04	...	...	5.31	0.00 ± 0.07	...
72	0.72 ± 0.02	−1.38 ± 0.02	−0.94 ± 0.02	3.28	0.60 ± 0.05	8.39
73	0.64 ± 0.01	...	...	3.38	0.47 ± 0.03	...
74	0.73 ± 0.01	−1.56 ± 0.02	−1.10 ± 0.02	3.42	0.32 ± 0.03	8.32
75	0.83 ± 0.04	−1.35 ± 0.03	−0.80 ± 0.02	3.29	0.60 ± 0.09	8.40

Figures 4 and 5 show [O III]/Hβ and [N II]/[O III] as a function of galactocentric distance in NGC 2366 and NGC 4395. These line ratios have *no* trend as a function of galactocentric distance in either galaxies.

4. DISCUSSION

The global changes of [O III]/Hβ, ([O II] + [O III])/Hβ, [N II]/[O III], and of other diagnostic line ratios across the disks of large spirals are driven primarly by abundance changes as a function of galactocentric distances (Searle 1971). Such ratios can be used to guess abundances where T_e-sensitive lines like [O III] λ4363 are too weak to be detected (Edmunds 1989). The use of these abundance indicators and their limitations has been discussed extensively by Stasińska et al. (1981), Edmunds & Pagel (1984), McCall et al. (1985), and Dopita & Evans (1986), and more recently by McGaugh (1991) and Zaritsky (1992). These ratios are sensitive also to properties like the effective temperature of the ionizing stars and to the ionization parameter. Following a thorough investigation of H II region photoionization models, McGaugh (1991) concluded that [O III]/Hβ alone is not a good metallicity indicator compared with ([O II] + [O III])/Hβ or [N II]/[O III]. Although Zaritsky, Elston, & Hill (1990) and Zaritsky (1992) showed that this ratio can track abundance variations in large disk galaxies when large samples of H II regions are available, this use becomes questionable in low-mass galaxies which tend to be relatively metal poor. We address first the issue of the

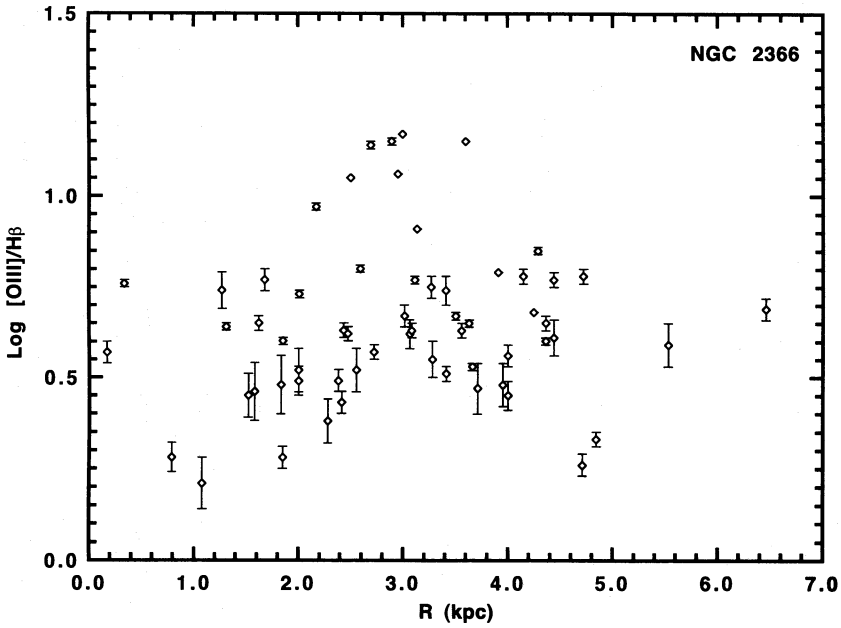

FIG. 4*a*

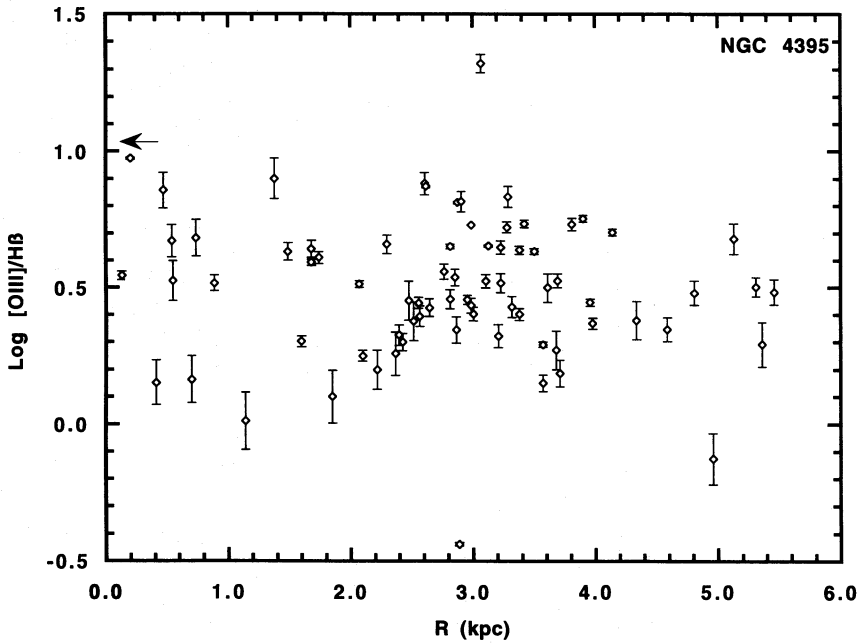

FIG. 4*b*

FIG. 4.—The quantity log [O III]/Hβ as a function of galactocentric distance in (*a*) NGC 2366 and (*b*) NGC 4395

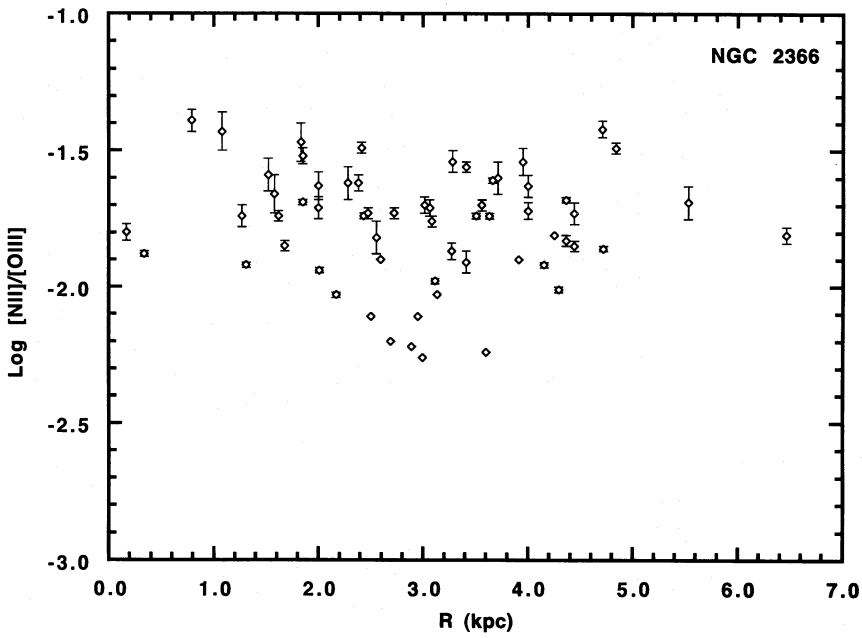

FIG. 5a

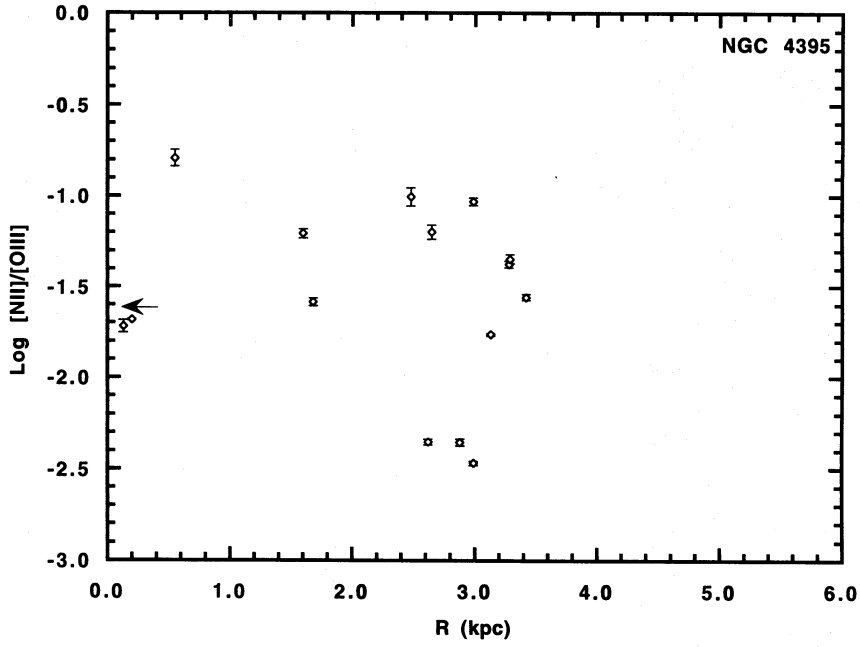

FIG. 5b

FIG. 5.—The quantity log [N II]/[O III] as a function of galactocentric distance in (*a*) NGC 2366 and (*b*) NGC 4395

reliability of [O III]/Hβ as an abundance indicator in low-mass galaxies, since NGC 2366 and NGC 4395 belong to this class.

4.1. [O III]/Hβ *as an Abundance Indicator*

The temperature in an H II region is determined by the equilibrium between heating (Γ) and cooling (Λ) rates (Osterbrock 1989). The energy input is due to photoionization, and the main energy loss is due to radiation of the heated gas. Of the many elements contributing to thermal balance, oxygen is the dominant cooling agent through the visible and infrared lines emitted by O^+ and O^{++}. The ratio [O III]/Hβ is sensitive to abundances for quite a range of abundances, but it is *not* sensitive for a limited domain around 12 + log O/H $\sim$ 8.4. Let us see why.

In the low-density limit, the strength of [O III]/Hβ is given by

$$[\mathrm{O\ III}]/\mathrm{H}\beta \propto \frac{\mathrm{O}^{++}}{\mathrm{H}}\, T^{(-0.5+m)} e^{-E_0/kT}, \qquad (1)$$

where E_0 is the excitation energy for the optical [O III] lines (Osterbrock 1989); the exponent m described the T^{-m} dependence of recombination lines where $m = 0.90$ for Hβ. To follow qualitatively the behavior of the [O III] line through a given range of parameters, the *dominant* cooling source at the equilibrium temperature needs to be known.

For extragalactic H II regions photoionized by massive stars, one can distinguish three regimes from the behavior of the optical oxygen lines [O II] and [O III]. In the very low-abundance regime, the nebular temperature at equilibrium is high, and cooling is mainly due to collisionally excited Lyα emission from hydrogen. Thus, the cooling rate $\Lambda \equiv f(T)$, and the electron temperature of the gas is independent of O/H; therefore, [O III]/H$\beta \propto$ O/H. This behavior is found in very low-mass galaxies and corresponds to the "lower branch" of the diagram [O/H] versus [O III]/Hβ and ([O II] + [O III])/Hβ, i.e., for 12 + log O/H $\leq$ 8.1.

As O/H in the gas is increased, the equilibrium temperature of the nebula is lowered. The main cooling source shifts to the emission of the *optical* lines of [O II] λ3727 and [O III] $\lambda\lambda$4959, 5007, that is,

$$\Lambda \equiv \frac{\mathrm{O}}{\mathrm{H}} T^{-0.5} e^{-E_0/kT}; \quad (2)$$

thus, [O II]/Hβ and [O III]/H$\beta \propto \Gamma$ and are nearly *independent* of O/H. This corresponds to the region of the *turnover* in the calibration curves [O/H] versus [O III]/Hβ or ([O II] + [O III])/Hβ. The strength of [O II]/Hβ and [O III]/Hβ depends mostly on the effective temperature of the ionizing radiation field and on $\bar{U}$ (see Edmunds & Pagel 1984; McGaugh 1991). This can happen in the abundance range 8.1 $\leq$ 12 + log O/H $\leq$ 8.6. McGaugh (1994) warned that many H II regions are bunched into this area of the calibrating diagrams of [O III]/Hβ and ([O II] + [O III])/Hβ versus [O/H], creating an artificial crowding of values near 12 + log O/H $\sim$ 8.4.

Finally, at abundances close to solar and higher (12 + log O/H $\geq$ 8.6), the equilibrium temperature is low (assuming that densities remain low enough to restrict collisional de-excitation); the radiative losses are increasingly dominated by the oxygen *infrared* lines at 52 μm and 88 μm, and

$$\Lambda \equiv \frac{\mathrm{O}^{++}}{\mathrm{H}} T^{-0.5} e^{-E_{\mathrm{ir}}/kT}. \quad (3)$$

E_{ir} is the excitation energy of the O^{++} levels responsible for the infrared lines. As O/H increases, the electron temperature decreases. Then

$$[\mathrm{O\ III}]/\mathrm{H}\beta \propto \Gamma e^{-(E_0 + E_{\mathrm{ir}})/kT}. \quad (4)$$

This results in the diminishing of the ratio ([O III] $\lambda\lambda$4959, 5007)/Hβ, and increasing the strength of the infrared lines, as O/H increases; the presence of dust and density effects may complicate the situation further (Henry 1993; Oey & Kennicutt 1993). In large galaxies, in which the level of O/H is generally high across the disk, the intensity of [O III]/Hβ is observed to increase as one goes from the inner parts to the outer parts of the disk, reflecting the systematic increase of O/H as one approaches the center. The radial trend of [O III]/Hβ is generally very obvious, and this is because of the strong dependence of the strength of the collisionally excited [O III] lines on electron temperature. Indeed, the observed behavior of [O III]/Hβ in large spirals appears well constrained.

As one considers galaxies of lower mass, and thus of lower metallicity, one moves closer to, or even into, the turnover regime in which both ([O II] + [O III])/Hβ and [O III]/Hβ are unsensitive to O/H variations. This happens at log [O III]/H$\beta \sim$ 0.7–1.0 for H II regions with high values of $\bar{U}$ (McGaugh 1991). Several values of [O III]/Hβ observed in NGC 2366 and NGC 4395 are close or in this regime. Consequently, one cannot use [O III]/Hβ as an abundance indicator in this regime; metallicity is low enough that the strength of the [O III] lines stops changing with T_e, i.e., we may be in the turnover part of the curve log O/H versus [O III]/Hβ; any gradient would be lost in the spread as a result of variations of $\bar{U}$.

The behavior of [O III]/Hβ as a function of gas metal abundance is further complicated by the fact that the ratio depends, in addition, on the temperature of the ionizing radiation field, and on the ionization parameter $\bar{U}$ defined as

$$\bar{U} = \frac{3Q}{4\pi c N R_{\mathrm{S}}^2}, \quad (5)$$

where Q is the ionizing luminosity, and N the gas density; R_{S} is the Strömgren radius ($R_{\mathrm{S}}^3 = 3Q/4\pi\epsilon\alpha N^2$), α being the hydrogen recombination coefficient for case B (Osterbrock 1989), and ϵ is the filling factor. Photoionization models by McGaugh (1991) show that the dependence on $\bar{U}$ is particularly strong at low metallicity, and that the spread in $\bar{U}$ is the most important source of variation of [O III]/Hβ and ([O II] + [O III])/Hβ at constant metallicity in the case of *giant* H II regions (see McGaugh 1991). McGaugh (1991) simulations indicate that observations have favored high $\bar{U}$ objects at low metallicity. Furthermore, the ionizing spectrum is affected by the mass and the metallicity of the stars (McGaugh 1991; Maeder 1990).

Values of [O III]/Hβ smaller than $\sim$0.8 may belong to the upper branch (corresponding to 12 + log O/H $\geq$ 8.0), or to the lower branch (i.e., 12 + log O/H $\leq$ 8.0), if one assumes small dispersion in $\bar{U}$ between H II regions (see McGaugh 1991). To establish which branch of the semiempirical calibration curve to use, one can use the abundance indicator [N II]/[O III] of Alloin et al. (1979), which is not double-valued at low O/H (McGaugh 1994). We used the ratio [N II]/[O III] to derive O/H abundances using the semiempirical calibration of Edmunds & Pagel (1984) that we adjusted with following polynomial:[1]

$$12 + \log \mathrm{O/H} = 8.77 - 0.214x - 0.407x^2 + 0.406x^3 - 0.118x^4, \quad (6)$$

where the variable $x \equiv \log$ [O III]/[N II]. The [N II]/[O III] data (Tables 5 and 6) for the two galaxies are consistent with the O/H abundances being in the regime in which [O III]/Hβ may *not* be sensitive to abundance, i.e., we are probably near or, worst, in the turnover of the calibration sequence of [O III]/Hβ. Thus, based on the abundance regime indicated by [N II]/[O III], [O III]/Hβ may be degenerate to O/H abundances in NGC 2366 and NGC 4395.

These arguments are supported by existing spectroscopy. McCall et al. (1985) measured the strength of [O III] λ4363 in four large H II regions in NGC 4395; they derived 12 + log O/H = 8.11, 8.26, 8.33, and 8.28. Regions in common with McCall et al. in NGC 4395 are shown as open triangles in Figure 6*b*. For NGC 2363 in NGC 2366, values of 7.92 are deduced from direct T_e measurement by Peimbert et al.; values of 8.00 are found by Masegosa, Moles, & del Olmo (1991); and values of 7.89 are found by Kennicutt et al. (1980) and González-Delgado et al. (1994); these are less than the value of 8.65 of Hunter & Gallagher

[1] Applicable only for 12 + log O/H < 8.7 or log [N II]/[O III] > 0.18.

(1985), who used a spectrum of NGC 2363 with low S/N. These O/H values and their correspondingly high values of [O III]/Hβ are indicative of objects in the turnover of the calibration sequence for [O III]/Hβ and ([O II] + [O III])/Hβ.

Finally, one should note that shocks in the ionized gas can lead to substantial enhancements of λ4363 while leaving [O III] $\lambda\lambda$4959, 5007 unaffected (Peimbert, Sarmiento, & Fierro 1991; McGaugh 1991). The presence of shocks is very likely in at least one large H II region of our sample, NGC 2363, the large H II complex in NGC 2366. Roy et al. (1991, 1992) have found a superbubble in NGC 2363 expanding at 50 km s^{-1}; thus, the high value of T_e (15,000 K) derived by Kennicutt et al. (1980) and Peimbert et al. (1986) may have a contribution owing in part to shock heating. We suspect that the same considerations may apply to many of the large H II complexes observed for extragalactic O/H measurements. [O III]/Hβ is seen to vary across the H II region NGC 2363, the ratio being the largest at the center of the region. [O III] λ4363 is most easily measured when the oxygen lines are strong, and abundances are derived assuming isothermality. In models including temperature structure, the derived abundances are systematically higher by 0.1–0.2 dex than for zero temperature fluctuations (Campbell 1988; McGaugh 1991). Thus, the true mean abundance in NGC 2363 may be higher than 12 + log O/H $\approx$ 7.9, and shock heating may explain why the points associated with the large H II complex NGC 2363 deviate from the mean trend (Fig. 6*a*).

4.2. O/H *in Low-Mass Galaxies*

Figure 6 shows 12 + log O/H versus radius in NGC 2366 and NGC 4395, where we derived O/H from [N II]/[O III] using the calibration of Edmunds & Pagel (1984). Abundances appear not to vary across the disks of the two galaxies, i.e., *their global O/H abundance gradients are flat*, or very shallow.

We conclude that 12 + log O/H = 8.19 $\pm$ 0.14 in NGC 2366 and 12 + log O/H = 8.33 $\pm$ 0.25 in NGC 4395; this is derived by merely taking the average of all abundance points in Figures 6*a* and 6*b* (or Tables 5 and 6), with the 1 σ dispersion about the mean. The value for NGC 4395 is close to the mean of the four O/H values deduced from direct T_e measurements by McCall et al. (1985). We recall the uncertainties of $\sim$0.2 dex on individual abundance points derived from the semiempirical calibration. In the case of the [N II]/[O III] indicator, the nucleogenic status of nitrogen affects the calibration; see the excellent discussion of this point in Dopita & Evans (1986). Low-mass irregulars have N/O ratios systematically lower than massive disk galaxies at a given O abundance. At low abundances, both primary and secondary processes appear to contribute to the nitrogen enrichment. However, we would certainly not claim that the scatter is driven by the varying enrichment origin of nitrogen. Instead, the observed scatter is probably dominated by experimental errors (e.g., due to the difficulty of measuring the weak [N II] line).

Few galaxies have been sampled well enough to state with certainty that they have no global radial abundance gradient. The Large Magellanic Cloud (LMC) shows a small negative O/H gradient, but the data are also consistent with no gradient at all (Pagel et al. 1978). The mean level of metals and the presence of a gradient appear related to some of the global properties of galaxies like the mass; however, the relationship between the mean level of metals and total mass or luminosity appears to break down at low galaxy mass and luminosity (McGaugh 1994).

Estimates of the total mass of the LMC differ; they vary from $\sim 6 \times 10^9\ M_\odot$ (Meatheringham et al. 1988) to $\geq 1.5 \times 10^{10}\ M_\odot$ (Schommer et al. 1992); the latter value is similar to that of NGC 4395 ($\sim 2 \times 10^{10}\ M_\odot$ from Wevers et al. 1986). The mass of NGC 2366 is small at $3 \times 10^9\ M_\odot$. The mean abundance level in the LMC is 12 + log O/H $\approx$ 8.4. The Small Magellanic Cloud, a much smaller galaxy than NGC 4395, does not have a gradient either, and the mean level of 12 + log O/H $\approx$ 8.0 (Pagel et al. 1978). NGC 55 is also another small galaxy with no apparent gradient (Webster & Smith 1983); however, NGC 55 is seen almost edge-on, and its gradient is not very reliable because of the very few points (eight H II regions) and of the large uncertainties in the deprojected radial distances of the H II regions. To summarize, although one cannot exclude the presence of negative O/H gradients in NGC 2366 and NGC 4395, they appear shallow enough to be lost in the dispersion intrinsic to the calibrators. Consequently, we surmise that the global O/H gradients in low-mass galaxies, such as the Magellanic Clouds, NGC 6288, NGC 2366, and NGC 4395, are flat or very shallow compared to those found in large spirals without bars. Finally, further spectroscopic study with several measurements of the [O III] λ4363 line would help to confirm our findings.

4.3. *The Origin of Shallow Abundance Gradients*

In the simple closed box model of galaxy evolution with no flow, the radial behavior of metallicity follows the stellar light distribution. The metallicity is given by $Z = p \ln(1/f)$, where f is the ratio of the gas mass density to total mass density and p is the yield. Since f generally increases with radius, this leads to a negative abundance gradient (as seen in normal spirals). Wevers et al. (1986) present the H I mass-to-(J) light ratio radial profiles of NGC 2366 and NGC 4395; although the ratio appears constant for the inner $\sim$1′, it *increases* with radial distance in NGC 2366 (for $R \geq 1.4$ kpc) and NGC 4395 (for $R \geq 1.1$ kpc). Thus, the simple model cannot be applied to low-mass or magellanic irregulars. One must find ways to produce shallow or flat global abundance gradients in such galaxies by introducing radial flows of interstellar gas.

4.3.1. *A Bar for Wiping Out Abundance Gradients*

While the presence of a bar in NGC 2366 is obvious, it is less so in NGC 4395, which is generally classified as a "normal" spiral (Sc or Sd). However, Martin & Roy (1994) and Martin (1995) have shown that a bar structure is present in NGC 4395; the bar is obvious in the red image of NGC 4395 (Fig. 2). Apart from its lower surface brightness, this galaxy is very similar to NGC 925 and NGC 1313 which are "barred" galaxies. Edmunds & Roy (1993) have already noted that abundance gradients seem to disappear at the same absolute magnitude ($M_B \sim -17$ in late-type spirals) where spiral structure no longer exists.

When a bar is present, angular momentum is removed from the interstellar gas and given up to the stellar population creating the nonaxisymmetric potential (Selwood & Wilkinson 1993) or to the spiral arms (Friedli, Benz, & Kennicutt 1994), and gas inflow and outflow take place. Thus, the presence of a bar is thought to be an effective way for radial homogenization of abundances (Pagel et al. 1978,

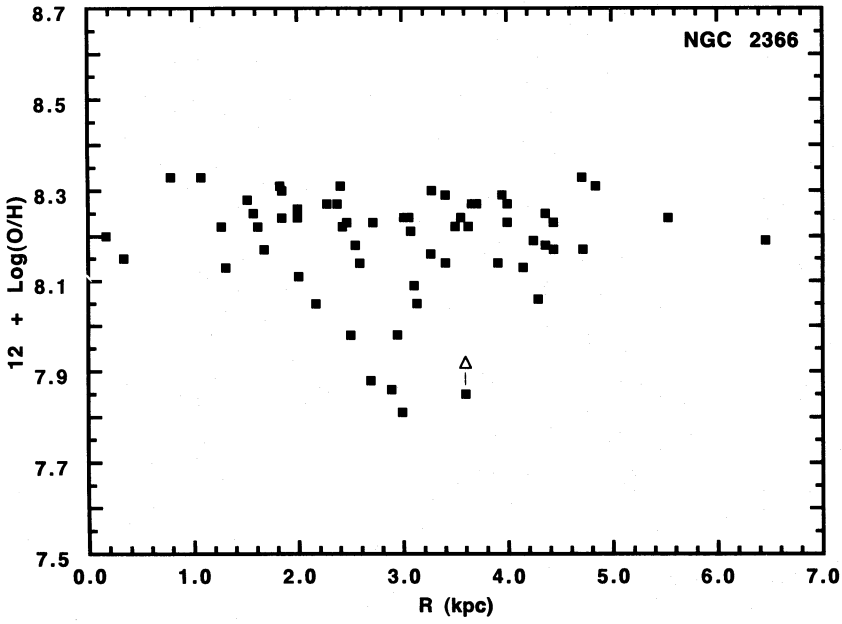

FIG. 6*a*

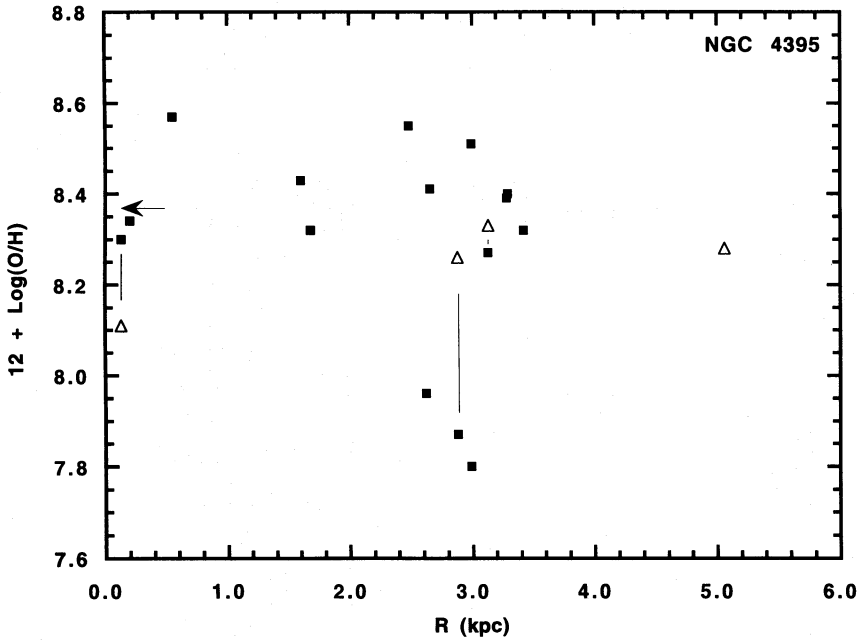

FIG. 6*b*

FIG. 6.—The quantity log 12 + log O/H as a function of galactocentric distance in (*a*) NGC 2366 and (*b*) NGC 4395. For NGC 4395, the open triangles correspond to the O/H abundances derived by McCall et al. (1985) from direct temperature measurements; the triangle for NGC 2366 is the measurement by Peimbert et al. (1986).

1979; Alloin et al. 1981; Lacey & Fall 1985; Edmunds 1990; Struck-Marcell 1991; Roy & Belley 1993; Martin 1992; Martin & Roy 1994; Friedli et al. 1994). These ideas are supported by the observation of strong noncircular motions in magellanic irregulars (Marcelin & Athanassoula 1982; Duval et al. 1991). However, with a young bar, vigorous star formation along the bar may compensate for the dilution effect of radial flows and maintain an existing gradient (Friedli et al. 1994; Martin & Roy 1995). Consequently, abundance gradients can be made shallower or steeper or be unaffected by a radial flow as demonstrated by Edmunds & Greenhow (1995); for the special case of a star formation law of the form $k(r)\rho^n$, with k constant and $n = 1$, it is shown that *no* abundance gradient will be generated in the gas for almost any initial gas configuration and any radial flow.

4.3.2. *Infall of Intergalactic Gas*

Infall of interstellar matter could have an important effect on the dynamical structure and chemical evolution of a spiral galaxy as demonstrated by Mayor & Vigroux (1981), Pitts & Tayler (1989), and Taylor (1990). Actually, most studies of the effect of infall have been conducted to explain

the strong abundance gradients that result from the accretion of external gas with low angular momentum. Mayor & Vigroux have shown that if the angular momentum of the infalling gas is zero with respect to the rotation axis, then a radial *inflow* is driven as a result of contraction of the disk because of conservation of angular momentum. In the more realistic case of oblique accretion, the field of perturbed velocities can be locally directed toward any direction, but there exists a contraction independent of the azimuthal angle which produces a net inflow as in the pole-on case.

Numerical simulations have been done by Mayor & Vigroux (1981) and Pitts & Tayler (1989); in the case of infalling gas with angular momentum *equal* to that of the impacting zone, no radial flow takes place and the resulting abundance gradient is almost *flat*, and Z tend to $p/(p + 1)$, where p is the yield. For the case in which the angular momentum of the infalling gas would be greater than that of the gas in the impacting zone, Pitts & Tayler suggest that the gradient would be even flatter, probably because of the radial outflow arising from angular momentum conservation. Undoubtedly models such as those of Pitts & Tayler, using the prescriptions of Edmunds & Greenhow (1995), could be run with a set of parameters capable of reproducing the mean level of O/H, the gas mass fraction, and the abundance distribution observed in NGC 2366 and NGC 4395. Again, as emphasized by Edmunds & Greenhow, gas flows can set up any gas and star distribution one wants, with no abundance gradient.

5. SUMMARY

A survey of O/H abundances employing imaging spectrophotometry with interference filters has been conducted of two low-mass galaxies: NGC 2366, a magellanic irregular, and NGC 4395, a small spiral with chaotic spiral structure. As expected for low-mass galaxies, the mean levels of O/H are moderately low, $12 + \log \mathrm{O/H} \approx 8.19 \pm 0.14$ in NGC 2366 and 8.33 ± 0.25 in NGC 4395 (where $\pm$ is the dispersion). There is *no* global O/H abundance gradient across the disks of the two galaxies. The absence of a metallicity gradient may be best explained by the large-scale redistribution of interstellar matter over the timescale of a few galactic rotations through the action of radial flows maintained by bars in the disks of those galaxies, and by the relatively uniform star formation rate across the disk over a large fraction of the galaxy lifetimes.

We held stimulating discussions with G. Stasińska, M. G. Edmunds, M. L. McCall, D. Kunth, and E. Hardy. We acknowledge the technical support of Bernard Malenfant and Ghislain Turcotte, the night assistants of Mont Mégantic Observatory. The Mont Mégantic Observatory is funded by the Natural Sciences and Engineering Research Council of Canada and by the Fond FCAR of the Government of Québec. The research of J. R. R. is funded by the Natural Sciences and Engineering Research Council of Canada.

REFERENCES

Alloin, D., Collin-Souffrin, S., Joly, M., & Vigroux, L. 1979, A&A, 78, 200
Alloin, D., Edmunds, M. G., Linblad, P. O., & Pagel, B. E. J. 1981, A&A, 101, 377
Belley, J., & Roy, J.-R. 1992, ApJS, 78, 61
Brocklehurst, M. 1971, MNRAS, 153, 471
Campbell, A. 1988, ApJ, 335, 644
de Vaucouleurs, G., de Vaucouleurs, A., Corwin, H. G., Buta, R. J., Paturel, G., & Fouqué, P. 1991, Third Reference Catalogue of Bright Galaxies (New York: Springer-Verlag)
Díaz, A. I. 1989, in Evolutionary Phenomena in Galaxies, ed. J. E. Beckman & B. E. J. Pagel (Cambridge: Cambridge Univ. Press), 377
Dinerstein, H. L. 1990, in The Interstellar Medium in Galaxies, ed. H. A. Thronson & J. M. Shull (Dordrecht: Kluwer), 257
Dopita, M. A., & Evans, I. N. 1986, ApJ, 307, 431
Dressel, L. L., & Condon, J. J. 1976, ApJS, 31, 187
Dufour, R. J. 1986, PASP, 98, 1025
Duval, M. F., Monnet, G., Boulesteix, J., Georgelin, Y., Le Coarer, E., & Marcelin, M. 1991, A&A, 241, 375
Edmunds, M. G. 1989, in Evolutionary Phenomena in Galaxies, ed. J. E. Beckman & B. E. J. Pagel (Cambridge: Cambridge Univ. Press), 356
———. 1990, MNRAS, 246, 678
Edmunds, M. G., & Greenhow, R. M. 1995, MNRAS, 272, 241
Edmunds, M. G., & Pagel, B. E. J. 1984, MNRAS, 211, 507
Edmunds, M. G., & Roy, J.-R. 1993, MNRAS, 261, L17
Elmegreen, B. G., & Elmegreen, D. M. 1987, ApJ, 314, 3
Filippenko, A. V., & Sargent, W. L. W. 1989, ApJ, 342, L11
Friedli, D., Benz, W., & Kennicutt, R. C. 1994, ApJ, 430, L105
González-Delgado, R. M., et al. 1994, ApJ, 437, 239
Henry, R. B. C. 1993, MNRAS, 261, 306
Henry, R. B. C., & Howard, J. W. 1995, ApJ, 438, 170
Hunter, D. A., & Gallagher, J. S. 1985, ApJS, 58, 533
Kennicutt, R. C., Balick, B., & Heckman, T. 1980, PASP, 92, 134
Lacey, C. G., & Fall, S. M. 1985, ApJ, 290, 154
Maeder, A. 1990, A&AS, 84, 139
Marcelin, M., & Athanassoula, E. 1982, A&A, 105, 76
Martin, P. 1992, Ph.D. thesis, Université Laval
———. 1995, AJ, 109, 2428
Martin, P., & Roy, J.-R. 1992, ApJ, 397, 463
———. 1994, ApJ, 424, 599
———. 1995, ApJ, 445, 161
Masegosa, J., Moles, M., & del Olmo, A. 1991, A&A, 249, 505
Mayor, M., & Vigroux, L. 1981, A&A, 98, 1
McCall, M. L. 1982, Ph.D. thesis, Univ. Texas, Austin
McCall, M. L., Rybski, P. M., & Shields, G. A. 1985, ApJS, 57, 1
McGaugh, S. S. 1991, ApJ, 380, 140
———. 1994, ApJ, 426, 135
Meatheringham, S. J., Dopita, M. A., Ford, H. C., & Webster, B. L. 1988, ApJ, 327, 651
Oey, M. S., & Kennicutt, R. C. 1993, ApJ, 411, 137
Osterbrock, D. E. 1989, Astrophysics of Gaseous Nebulae and Active Galactic Nuclei (Mill Valley: University Science Books)
Pagel, B. E. J., & Edmunds, M. G. 1981, ARA&A, 19, 77
Pagel, B. E. J., Edmunds, M. G., Blackwell, D. E., Chun, M. S., & Smith, G. 1979, MNRAS, 189, 95
Pagel, B. E. J., Edmunds, M. G., Fosbury, R. A. E., & Webster, B. L. 1978, MNRAS, 184, 569
Pagel, B. E. J., Edmunds, M. G., & Smith, G. 1980, MNRAS, 193, 219
Peimbert, M., Pena, M., & Torres-Peimbert, S. 1986, A&A, 158, 266
Peimbert, M., Sarmiento, A., & Fierro, J. 1991, PASP, 103, 815
Pitts, E., & Tayler, R. J. 1989, MNRAS, 240, 373
Roy, J.-R., Aubé, M., McCall, M. L., & Dufour, R. J. 1992, ApJ, 386, 498
Roy, J.-R., & Belley, J. 1993, ApJ, 406, 60
Roy, J.-R., Boulesteix, J., Joncas, G., & Grundseth, B. 1991, ApJ, 367, 141
Ryder, S. D. 1995, ApJ, 444, 610
Sandage, A., & Tammann, G. A. 1981, A Revised Shapley-Ames Catalog of Bright Galaxies (Washington: Carnegie Institution of Washington)
Savage, B. D., & Mathis, J. S. 1979, ARA&A, 17, 73
Schommer, R. A., Olszewski, E. W., Suntzeff, N. B., & Harris, H. C. 1992, AJ, 103, 447
Scowen, P. A., Dufour, R. J., & Hester, J. J. 1992, AJ, 104, 92
Searle, L. 1971, ApJ, 168, 327
Selwood, J. A., & Wilkinson, A. 1993, Rep. Prog. Phys., 56, 173
Shields, G. A. 1990, ARA&A, 28, 525
Skillman, E. D., Terlevich, R. J., Kennicutt, R. D., Garnett, D. R., & Terlevich, E. 1994, ApJ, 431, 172
Stasińska, G., Alloin, D., Collin-Souffrin, S., & Joly, M. 1981, A&A, 93, 362
Struck-Marcell, C. 1991, ApJ, 368, 348
Tayler, R. C. 1990, QJRAS, 31, 281
Tully, R. B. 1988, Nearby Galaxies Catalog (Cambridge: Cambridge Univ. Press)
Vila-Costas, M. B., & Edmunds, M. G. 1992, MNRAS, 259, 121
van der Hults, J. M., Kennicutt, R. C., Crane, P. C., & Rots, A. H. 1988, A&A, 195, 38
Walsh, J. R., & Roy, J.-R. 1989a, ApJ, 341, 722
———. 1989b, MNRAS, 239, 297
———. 1993, MNRAS, 262, 27
Webster, L. B., & Smith, M. G. 1983, MNRAS, 204, 743
Wevers, B. M. H. R., van der Kruit, P. C., & Allen, R. J. 1986, A&AS, 66, 505
Zaritsky, D. 1992, ApJ, 390, L73
Zaritsky, D., Elston, R., & Hill, J. M. 1990, AJ, 99, 1108
Zaritsky, D., Kennicutt, R. C., & Huchra, J. P. 1994, ApJ, 420, 87